Published in final edited form as:

Science. 2023 August 18; 381(6659): 754–760. doi:10.1126/science.adg7731.

Design of stimulus-responsive two-state hinge proteins

Florian Praetorius[†,*,1,2], **Philip J. Y. Leung**[†,1,2,3], **Maxx H. Tessmer**[4], **Adam Broerman**[1,2,5], **Cullen Demakis**[1,2,6], **Acacia F. Dishman**[1,2,7,8], **Arvind Pillai**[1,2], **Abbas Idris**[1,2,9], **David Juergens**[1,2,3], **Justas Dauparas**[1,2], **Xinting Li**[1,2], **Paul M. Levine**[1,2], **Mila Lamb**[1,2], **Ryanne K. Ballard**[1,2], **Stacey R. Gerben**[1,2], **Hannah Nguyen**[1,2], **Alex Kang**[1,2], **Banumathi Sankaran**[10], **Asim K. Bera**[1,2], **Brian F. Volkman**[7], **Jeff Nivala**[11,12], **Stefan Stoll**[4], **David Baker**[*,1,2,13]

[1.]Department of Biochemistry, University of Washington, Seattle, WA, USA.

[2.]Institute for Protein Design, University of Washington, Seattle, WA, USA.

[3.]Graduate Program in Molecular Engineering, University of Washington, Seattle, WA, USA.

[4.]Department of Chemistry, University of Washington, Seattle, WA, USA.

[5.]Department of Chemical Engineering, University of Washington, Seattle, WA, USA.

[6.]Graduate Program in Biological Physics, Structure, and Design, University of Washington, Seattle, Washington, USA.

[7.]Department of Biochemistry, Medical College of Wisconsin, Milwaukee, WI, USA.

[8.]Medical Scientist Training Program, Medical College of Wisconsin, Milwaukee, WI, USA.

[9.]Department of Bioengineering, University of Washington, Seattle, WA, USA.

[10.]Molecular Biophysics and Integrated Bioimaging, Lawrence Berkeley National Laboratory, Berkeley, CA, USA

[*]Corresponding author flop@uw.edu, dabaker@uw.edu.
[†]These authors contributed equally to this work

Author contributions

F.P. developed the hinge design concept. F.P. and P.J.Y.L. developed the computational hinge design pipeline. F.P. and P.J.Y.L. designed, screened, and characterized most hinges with help from C.D. and A.P.. M.H.T. designed, performed and analyzed DEER experiments. S.S. analyzed DEER data and supervised research. C.D. developed the one-sided two-state design protocol and designed and tested hinges with swapped targets. A.B. designed and characterized 3-helix bundles with support from D.C.J.. A.I. designed and characterized the hinge-armed trimer with support from A.B.. A.I. performed electron microscopy and image processing with support from A.P.. J.D. provided conceptual support for two-state sequence design. X.L., P.M.L., M.L., and R.K.B. synthesized and purified peptides. X.L., M.L., and R.K.B. performed LC-MS validation of proteins and peptides. S.R.G. performed additional protein purification. H.N., A.K., B.S., and A.K.B. determined crystal structures. A.F.D. and B.V. contributed conceptual support. D.B. and J.N. supervised research. F.P., P.J.Y.L., and D.B. wrote the manuscript. M.H.T. contributed to the manuscript. All authors read and commented on the manuscript.

Competing interests

A provisional patent application will be filed prior to publication, listing F.P., P.J.Y.L., M.H.T., A.B., C.D., A.F.D., A.P., A.I., B.V., S.S., and D.B. as inventors or contributors.

Data and materials availability

All data are available in the main text or as supplementary materials. Design models are available in supplementary file S2 and through Zenodo (41). Design scripts are available in supplementary file S3 and through Zenodo (41). Raw DEER data are available through Zenodo (41). Crystallographic datasets have been deposited in the Protein Data Bank (PDB) (accession codes 8FIH, 8FVT, 8FIT, 8FIN and 8FIQ).

[11.]Paul G. Allen School of Computer Science and Engineering, University of Washington, Seattle, WA, USA.

[12.]Molecular Engineering and Sciences Institute, University of Washington, Seattle, WA, USA.

[13.]Howard Hughes Medical Institute, University of Washington, Seattle, WA,USA.

Abstract

In nature, proteins that switch between two conformations in response to environmental stimuli structurally transduce biochemical information in a manner analogous to how transistors control information flow in computing devices. Designing proteins with two distinct but fully structured conformations is a challenge for protein design as it requires sculpting an energy landscape with two distinct minima. Here we describe the design of “hinge” proteins that populate one designed state in the absence of ligand and a second designed state in the presence of ligand. X-ray crystallography, electron microscopy, double electron-electron resonance spectroscopy and binding measurements demonstrate that, despite the significant structural differences, the two states are designed with atomic level accuracy and that the conformational and binding equilibria are closely coupled.

One Sentence Summary:

Two-state design of protein switches that couple effector binding to a conformational change

---

While many naturally occurring proteins adopt single folded states, conformational changes between distinct protein states are crucial to the functions of enzymes(1, 2), cell receptors(3), and molecular motors(4). The extent of these changes ranges from small rearrangements of secondary structure elements(5, 6) to domain rearrangements(7) to fold-switching or metamorphic proteins(8) that adopt completely different structures. In many cases, these conformational changes are triggered by “input” stimuli such as binding of a target molecule, post-translational modification, or change in pH. These changes in conformation can in turn result in “output" actions such as enzyme activation, target binding, or oligomerization(9); protein conformational changes can thus couple a specific input to a specific output. The generation of proteins that can switch between two quite different structural states is a difficult challenge for computational protein design, which usually aims to optimize a single, very stable conformation to be the global minimum of the folding energy landscape(10, 11). Design of such proteins requires reframing the design paradigm towards optimizing for more than one minimum on the energy landscape, while simultaneously avoiding undesired off-target minima(12). Previously, multi-state design has been used to design proteins that undergo very subtle conformational changes(13, 14), cyclic peptides that switch conformations based on the presence of metal ions(15), and closely related sequences that fold into dramatically different conformations(16). Stimulus-responsive “LOCKR” proteins have been designed to undergo conformational changes upon binding to a target peptide or protein(17); however, while the “closed” unbound state of these “switch” proteins is a well-defined and fully structured conformation, the “open” bound state is a broad distribution of conformations. The LOCKR platform has been used to

generate biosensors(18, 19), but the lack of a defined second state makes it not well suited for mechanical coupling in a molecular machine or discrete state-based computing systems.

Hinge Design Method

We set out to design proteins that can switch between two well-defined and fully structured conformations. To facilitate experimental characterization of the conformational change and to ensure compatibility with downstream applications, we imposed several additional requirements. First, the conformational change between the two states should be large, with some inter-residue distances changing by tens of angstroms between the two states. Second, the conformational change should not require global unfolding, which can be very slow. Third, neither of the two states should have substantial exposed patches of hydrophobic residues, which can compromise solubility. Fourth, the conformational change should be readily coupled to a range of inputs and outputs. Given that proteins are stabilized by hydrophobic cores, collectively achieving all of these properties in one protein system is challenging: protein conformations that differ considerably typically will have different sets of buried hydrophobic residues and require substantial structural rearrangements for interconversion.

We reasoned that these goals could be collectively achieved with a “hinge”-like design in which two rigid domains move relative to each other while remaining individually folded. The hinge amplifies small local structural and chemical changes to achieve large global changes while the chemical environment for most residues remains similar throughout the conformational change, avoiding the need for global unfolding. Provided that the two states of the hinge bury similar sets of hydrophobic residues, the amount of exposed hydrophobic surface area can be kept low in both states. Designing one of the resulting conformations to bind to a target effector couples the conformational equilibrium with target binding (Figure 1A). This design concept has precedent in nature; for example bacterial two-component systems utilize binding proteins that undergo hinging between two discrete conformations in response to ligand binding(20).

To implement this two-state hinge design concept, we took advantage of designed helical repeat proteins (DHRs, (21); Figure 1B,C left) and DHR-based junction proteins(22). The backbone conformation of the DHR serves as the first conformational state of our hinge protein (“state X”). To generate a second conformation, a copy of the parent protein is rotated around a “pivot helix” (Figure 1B,C) and a new backbone conformation is then created by combining the first half of the original protein (domain 1), the second half of the copy (domain 2), and either the helix following the pivot helix from the original protein or the helix preceding the pivot helix from the rotated copy (“peptide”). Rosetta FastDesign with backbone movement(23, 24) is used to re-design the interface between the three parts, and the two domains are connected into a single chain using fragment-based loop closure(21, 25, 26). Using a combination of Rosetta two-state design (see methods section for details) and proteinMPNN(27) with linked residue identities, a single amino acid sequence is generated that is compatible with the state X hinge as well as with the state Y hinge-peptide complex. AlphaFold2 (AF2)(28) with initial guess(29) is then used to predict the structure of the hinge with and without the effector peptide, allowing for the selection of

designs that are predicted in the correct state X in absence of the peptide and in the correct state Y complex in presence of the peptide. To favor designs that are predominantly in the closed state in absence of the peptide (Figure 1A,D), designs are selected only if state X has lower energy (computed using Rosetta) than state Y in absence of the peptide, and if the state Y complex has lower energy than state X plus spatially separated peptide. Designs are also filtered on standard interface design metrics for the bound conformation (see Methods for details on filtering)(30).

Hinges bind effector peptides with sub-nM to low μM affinities

We used our hinge design approach to generate hinge-peptide pairs that span a wide structural space (Figures 1D, 2A, S1, S2). We experimentally tested multiple rounds of designs, using both DHRs(21) and helical junctions(22) as input scaffolds, and improving individual steps of the design pipeline between iterations (see Supplementary Note 1 for details on screening and a discussion of success rates and failure modes). Designs for which hinge and GFP-fused peptide were soluble and interacted as judged by size exclusion chromatography (SEC, Figures S2,S3) were selected for further characterization by fluorescence polarization (FP). Hinge-peptide binding affinities obtained from FP titration experiments with constant peptide concentration and varying hinge concentrations ranged from 1 nM to the low μM range (Figures 2B, S4, Table S1). To circumvent the bottleneck of finding soluble peptide sequences (see Supplementary Note 1), we also sought to design hinges that bind to a given target peptide. Starting from design cs201, we used a modified version of our design pipeline to redesign the hinge to bind peptides cs074B or cs221B, respectively, which have similar hydrophobic fingerprints as the original target peptide cs201B. This one-sided two-state design approach yielded hinge designs that showed strong binding to their new target peptide while showing no or only weak off-target binding (Figure S5).

Effector binding modulates the hinge conformational equilibrium

To characterize the conformational equilibrium of the designed hinges, we introduced two surface cysteine residues into the hinge protein and covalently labeled them with the nitroxide spin label MTSL(31). We then used double electron-electron resonance spectroscopy (DEER) to determine distance distributions between the two spin labels and compared these to simulated(32) distance distributions based on the state X and state Y design models. This experiment was performed on two different labeling site pairs for each design: one pair where the distance is predicted to decrease in the presence of peptide (Figures 2C, S4C,D) and the other where it is predicted to increase (Figures 2D, S4C,D). In the absence of the peptide, the observed distance distributions closely matched the state X simulations. In all cases the distances between the two pairs of probes shifted upon addition of peptide to better match the state Y simulations, suggesting that addition of effector peptide causes the conformational equilibrium to shift towards state Y as designed. For example, cs074 (site pair 1) showed a clear peak between 40 and 50 Å in absence of the peptide, and a peak between 30 and 40 Å in presence of the peptide, and both peaks agree well with the corresponding simulations (Figure 2C, top row). In a control experiment using the static parent DHR protein of design cs074, the distance distributions with and without

peptide were identical and matched both the simulation for the parent design model, which closely resembles state X, and the experimental distance distribution for state X of cs074 (Figure S4D).

We solved crystal structures for two designs, cs207 and cs074. For design cs207, crystals were obtained from two separate crystallization screens: one screen for the hinge alone, and one screen for the hinge in complex with the target peptide. In the absence of peptide the experimental structure agrees well with the state X design model (Figure 3A), and the structure of the hinge-peptide complex agrees well with the state Y design model (Figure 3B). The crystal structures of hinge cs207 in both designed states demonstrate the accuracy with which two very different conformational states of the same protein can now be designed. For design cs074, the crystal structure of the hinge-peptide complex agrees well with the corresponding state Y design model (Figure 3C).

One major advantage of de novo designed proteins is their robustness to external conditions, such as high temperatures, and to structural perturbations, such as mutations, genetic fusion, and incorporation in designed protein assemblies. Circular Dichroism (CD) melts show that our hinges remain folded at high temperatures (Figure S6), like the DHRs they were based on(21). To test whether our hinges can be incorporated as components of more complex protein assemblies without affecting their ability to undergo conformational changes, we designed a fully structured C3-symmetric protein with three hinge arms (Figure 3D). We used inpainting(33) with RoseTTAFold(34) to rigidly connect one end of hinge cs221 to a previously validated homotrimer(35, 36) and the other end of the hinge to a previously validated monomeric protein(37). Negative-stain electron microscopy (nsEM) with reference-free class averaging shows straight arms in absence of peptide and bent arms in presence of peptide cs221B, corroborating the designed conformational change (Figures 3D, S7).

A critical feature of two-state switches in biology and technology is the coupling between the state control mechanism and the populations of the two states. To quantitatively investigate the thermodynamics and kinetics of the effector induced switching between the two states of our designed hinges, we used Förster resonance energy transfer (FRET). To increase both the absolute distance from N- to C- terminus and the change in termini distance between the two conformational states, we took advantage of the extensibility of repeat proteins and extended hinges cs074, cs221, and cs201 by 1-2 helices on their N and C termini, yielding cs074F, cs221F, and cs201F, respectively (Figure 4A, first column). Single cysteines were introduced in helical regions near the termini of the extended hinges and stochastically labeled with an equal mixture of donor and acceptor dyes. For hinges cs074F and cs221F the distance between the label sites is above the R_0 of the dye pair in state X and below R_0 in state Y, and hence, acceptor emission upon donor excitation increases upon addition of the corresponding peptides cs074B and cs221B, respectively (Figure 4A, second column). We used labeled, extended DHR82, the parent protein for cs074F, as a static control, and observed fluorescence spectra comparable to cs074F but no change in fluorescence upon addition of the peptide (Figure S8A,B). For cs201F, the dye distance is above R_0 in state X and below R_0 in state Y, and donor emission decreases upon addition of peptide cs201B (Figure 4A, second column). To test specificity of our hinge-peptide pairs,

we performed pairwise titrations of all three labeled hinges at 2 nM with all three target peptides at varying concentrations. The on-target titrations had sigmoidal transitions that can be fitted with standard binding isotherms (Figures 4A, third column; S8C), whereas the off-target titrations for cs201F and cs221F show flat lines, indicating no conformational change of these hinges upon addition of off-target peptides at μM concentrations. cs074F showed weak off-target binding that was three orders of magnitude weaker for cs201B and two orders of magnitude weaker for cs221B compared to the on-target interaction for cs074B. cs201F and cs221F are thus orthogonal from the nM to the μM range, and the set of cs201F, cs221F, and cs074F is orthogonal over two orders of magnitude of effector concentration.

Association kinetics for the on-target interactions measured using constant concentrations of labeled hinge and varying excess concentrations of peptide are well fit by single exponentials (Figures 4A, fourth column; S9). The apparent rate constants increase linearly with increasing peptide concentration, exhibiting standard pseudo-first order kinetics for bimolecular reactions (Figures 4A, fifth column; S9). We analyze these data using a model comprising the three states (X, Y, Y+peptide) and four rate constants (Figure 4B). The kinetic measurements using the FRET system follow the decrease in state X over time (d[X]/dt) upon the addition of peptide. The observed pseudo-first order behavior (Figure 4A, fifth column) indicates that the conformational change happens on a timescale that is faster than that of the observed binding and can be treated as a fast pre-equilibrium (Supplementary Note 2). The slopes of the linear pseudo-first order fits (k_{on}) can thus be interpreted as the product of the microscopic association rate k_2 and the fractional population of state Y in absence of the peptide ($F_Y = [Y]/([X]+[Y])$, see Supplementary Note 2). FP based titrations and kinetic characterization using the unlabeled extended hinge cs074F in excess over the TAMRA-labeled peptide cs074B agree well with the corresponding FRET experiments, further supporting the pre-equilibrium model (Figures 4C, S9). FP kinetics experiments for other hinge designs also follow pseudo-first order behavior with k_{on} values ranging from $2.5x10^3$ $M^{-1}s^{-1}$ to $7.8x10^4$ $M^{-1}s^{-1}$ (Figures S4B, S10). To study the reversibility of hinge conformational changes, we started with 30 nM of FRET-labeled hinge cs201F (Figure 4D), added 200 nM peptide to drive the conformational change, and then added excess unlabeled hinge cs201 to compete away the peptide. The FRET signal decreased upon addition of the peptide, consistent with conformational change from state X to state Y, and then returned to nearly the original level upon addition of unlabeled hinge, indicating that the hinge conformational change is fully reversible.

To explore whether peptide-responsive hinges could be turned into protein-responsive hinges, we used inpainting with RoseTTAFold to add two additional helices to a validated effector peptide, resulting in fully structured 3-helix bundles (3hb). For nine of our validated hinges we designed and experimentally characterized these effector proteins using SEC (Figures 4E, S11A, S12). Hinge-3hb binding was tested qualitatively by SEC and, for hinges which had a corresponding FRET construct, quantitatively with the FRET-labeled variant, and DEER was used in addition to FRET to confirm that 3hb binding caused the same conformational change as effector peptide binding (Figures 4E, bottom; S11). The affinity of 3hb05 to cs074F was similar to the affinity observed for the original peptide cs074B (Figure 4E), whereas 3hb21 bound its target hinge cs221F significantly tighter than the original

peptide cs221B (Figure S13). The 3hb approach was able to rescue designs for which the peptide alone or the hinge-peptide complex had shown the tendency to form higher-order oligomers (Figure S12). For two designs, 3hb05 and 3hb12, we obtained crystal structures that agreed well with the design models, indicating that the three-helix bundles are fully structured in isolation (Figures 4E top right, S14).

The conformational pre-equilibrium controls effector binding

To test the effect of the conformational pre-equilibrium on effector binding, we introduced disulfide “staples” that lock the hinge in one conformation. Using FP we analyzed peptide binding to stapled versions of hinge cs221 (Figure 5A,B). The variant that forms a disulfide bond in state X (“locked X”) showed only weak residual binding, likely due to a small fraction of hinges not forming the disulfide (Figure 5A). Upon addition of the reducing agent dithiothreitol (DTT) to break the disulfide, peptide binding was fully restored, making this hinge variant a red/ox dependent peptide binder that binds the effector peptide under reducing but not under oxidizing conditions. The association rate for the locked Y variant was 200-fold higher than for the original hinge without disulfides (Figures 5B, S15A,B; despite this increase the overall binding affinity was weaker, suggesting the disulfide may lock the hinge in a slightly perturbed version of state Y). Using the pre-equilibrium model described above, the observed association rates provide an estimate of the fraction of hinge that is in state Y in absence of the peptide: a 200-fold higher observed on rate for the locked Y variant indicates a 200-fold higher fraction of hinge in state Y compared to the original hinge. Assuming that the locked Y variant is 100% in state Y and assuming that the microscopic rate constant k_2 is identical for the locked Y hinge and state Y of the original hinge, this would indicate that the original hinge is 99.5% in state X and 0.5% in state Y at equilibrium.

Having established the edge cases of locked state X and locked state Y, we sought to tune the pre-equilibrium by introducing single point mutations expected to specifically stabilize one state over the other while not directly affecting the peptide-binding interface. We used proteinMPNN to generate consensus sequences(38) for each state and identified non-interface positions with distinct residue preferences that were different between both states (Figures 5C, S16A). We experimentally tested individual protein variants carrying substitutions expected to stabilize one state over the other without disrupting either conformation, as evaluated by AF2 predictions. Consistent with coupling of the conformational and binding equilibria, substitutions based on state X consensus sequences led to weaker peptide binding, and those based on state Y consensus sequences led to stronger binding (Figures 5C, S15C). The substitutions that stabilized state Y showed accelerated association kinetics (Figures 5C, S17), consistent with our kinetic model (Figures 4B, S16B,C, Supplementary Note 2): the mutations effectively shift the conformational pre-equilibrium towards state Y, increasing the on rates. This close coupling of the conformational equilibrium with association kinetics further supports the model outlined in Fig 4B, and the fine tunability should be useful in downstream applications.

The state Y-stabilizing double mutant cs221_V111L_A114T has a 22-fold higher on rate than the original cs221, suggesting the occupancy of state Y in cs221_V111L_A114T is 22x

higher in the absence of peptide. Distance distributions obtained from DEER measurements on site pair 2 of the double mutant cs221_V111L_A114T in absence of the peptide indeed showed an additional peak at a distance closely matching state Y (Figures 5C, S18). DEER measurements on site pair 1 of the double mutant showed a broader distribution with occupancy in the region corresponding to state Y (Figures 5C, S18). Measurements in the presence of the peptide were virtually indistinguishable from the original cs221 (Figure S18). The double mutant thus populates two distinct states in the absence of the effector, and collapses to one state upon effector addition (Figures 5E, S18). The observation of a significant state Y population at equilibrium in the absence of the peptide as predicted based on the kinetic measurements further corroborates that the mutations affect the conformational pre-equilibrium, and provides strong support for our quantitative two-state model of the kinetics and thermodynamics of the designed hinge-effector systems.

Conclusion

Our hinge design method generates proteins that populate two well-defined and structured conformational states, rather than adopting a heterogenous mixture of structures, and should be broadly applicable to design of functional proteins. Like transistors in electronic circuits, we can couple the switches to external outputs and inputs to create sensing devices and incorporate them into larger protein systems to address a wide range of outstanding design challenges. Hinges containing a disulfide that locks them in state X couple the input “red/ox state” to the output “target binding,” where the target can be a peptide or a protein, and our FRET-labeled hinges couple the input “target binding” to the output “FRET signal.” Our approach can be readily extended such that state switching is driven by naturally occurring rather than designed peptides: recent designed extended peptide binding proteins (39) resemble the state X of our hinges, and recent designs that bind glucagon, secretin, or neuropeptide Y(40) resemble the state Y of our hinges. Hinges based on such designs could thus provide new routes to applications in sensing and detection.

Stimulus-responsive protein assemblies that switch between two well-defined shapes or oligomeric states in the presence of an effector can now be built by incorporating the hinges as modular building blocks, which was not possible with the previous LOCKR switches as one of the LOCKR states is disordered. Installing enzymatic sites in hinges such that substrate binding favors one state and product release favors the other state should enable fuel-driven conformational cycling, a crucial step towards the *de novo* design of molecular motors. More generally, the ability to design two-state systems, and the designed two-state switches presented here, should enable protein design to go beyond static structures to more complex multistate assemblies and machines.

Supplementary Material

Refer to Web version on PubMed Central for supplementary material.

Acknowledgements

We thank Basile I. M. Wicky, Lukas F. Milles, and Danny D. Sahtoe for helpful discussions and technical support, Alexis Courbet for inspiring discussions, Annika Philomin and Andrew Borst for EM support, and Kandise VanWormer and Luki Goldschmidt for technical support.

We want to thank the Advanced Light Source (ALS) beamline 8.2.2/8.2.1 at Lawrence Berkeley National Laboratory for X-ray crystallography data collection. The Berkeley Center for Structural Biology is supported in part by the National Institutes of Health (NIH), National Institute of General Medical Sciences, and the Howard Hughes Medical Institute. The ALS is supported by the Director, Office of Science, Office of Basic Energy Sciences and US Department of Energy (DOE) (DE-AC02-05CH11231).

Funding

This work was supported by a Human Frontier Science Program Long Term Fellowship (LT000880/2019, F.P.), the Open Philanthropy Project Improving Protein Design Fund (P.J.Y.L., C.W.D., H.N., D.B.), an NSF Graduate Research Fellowship (DGE-2140004; P.J.Y.L), NERSC award BER-ERCAP0022018 (P.J.Y.L, D.B.), the Audacious Project at the Institute for Protein Design (A.B., A.P., A.I., M.L., R.K.B., S.R.G., A.K., D.B.), a gift from Microsoft (D.J., J.D., D.B.), a grant from DARPA supporting the Harnessing Enzymatic Activity for Lifesaving Remedies (HEALR) program (HR001120S0052 contract HR0011-21-2-0012, X.L., A.K.B., D.B.), the Defense Threat Reduction Agency (DTRA) grant # HDTRA1-19-1-0003 (P.M.L.), NSF Award #2006864 (J.N.), and the Howard Hughes Medical Institute (D.B.). DEER measurements were supported by R01 GM125753 (to S.S.). The spectrometer used was funded by NIH grant S10 OD021557 (S.S.).

References

1. Stiller JB, Otten R, Häussinger D, Rieder PS, Theobald DL, Kern D, Structure determination of high-energy states in a dynamic protein ensemble. Nature. 603, 528–535 (2022). [PubMed: 35236984]
2. Kerns SJ, Agafonov RV, Cho Y-J, Pontiggia F, Otten R, Pachov DV, Kutter S, Phung LA, Murphy PN, Thai V, Alber T, Hagan MF, Kern D, The energy landscape of adenylate kinase during catalysis. Nat. Struct. Mol. Biol 22, 124–131 (2015). [PubMed: 25580578]
3. Bisello A, Chorev M, Rosenblatt M, Monticelli L, Mierke DF, Ferrari SL, Selective ligand-induced stabilization of active and desensitized parathyroid hormone type 1 receptor conformations. J. Biol. Chem 277, 38524–38530 (2002). [PubMed: 12107160]
4. Movassagh T, Bui KH, Sakakibara H, Oiwa K, Ishikawa T, Nucleotide-induced global conformational changes of flagellar dynein arms revealed by in situ analysis. Nat. Struct. Mol. Biol 17, 761–767 (2010). [PubMed: 20453857]
5. Catterall WA, Wisedchaisri G, Zheng N, The conformational cycle of a prototypical voltage-gated sodium channel. Nat. Chem. Biol 16, 1314–1320 (2020). [PubMed: 33199904]
6. Evans EGB, Morgan JLW, DiMaio F, Zagotta WN, Stoll S, Allosteric conformational change of a cyclic nucleotide-gated ion channel revealed by DEER spectroscopy. Proc. Natl. Acad. Sci. U. S. A 117, 10839–10847 (2020). [PubMed: 32358188]
7. Arragain B, Effantin G, Gerlach P, Reguera J, Schoehn G, Cusack S, Malet H, Pre-initiation and elongation structures of full-length La Crosse virus polymerase reveal functionally important conformational changes. Nat. Commun 11, 3590 (2020). [PubMed: 32681014]
8. Kim AK, Porter LL, Functional and Regulatory Roles of Fold-Switching Proteins. Structure. 29, 6–14 (2021). [PubMed: 33176159]
9. Ha J-H, Loh SN, Protein conformational switches: from nature to design. Chemistry. 18, 7984–7999 (2012). [PubMed: 22688954]
10. Huang P-S, Oberdorfer G, Xu C, Pei XY, Nannenga BL, Rogers JM, DiMaio F, Gonen T, Luisi B, Baker D, High thermodynamic stability of parametrically designed helical bundles. Science. 346, 481–485 (2014). [PubMed: 25342806]
11. Koga R, Yamamoto M, Kosugi T, Kobayashi N, Sugiki T, Fujiwara T, Koga N, Robust folding of a de novo designed ideal protein even with most of the core mutated to valine. Proc. Natl. Acad. Sci. U. S. A 117, 31149–31156 (2020). [PubMed: 33229587]

12. Dishman AF, Volkman BF, Design and discovery of metamorphic proteins. Curr. Opin. Struct. Biol 74, 102380 (2022). [PubMed: 35561475]
13. Joh NH, Wang T, Bhate MP, Acharya R, Wu Y, Grabe M, Hong M, Grigoryan G, De Grado WF, De novo design of a transmembrane Zn2+-transporting four-helix bundle.
14. Davey JA, Damry AM, Goto NK, Chica RA, Rational design of proteins that exchange on functional timescales. Nat. Chem. Biol 13, 1280–1285 (2017). [PubMed: 29058725]
15. Mulligan VK, Kang CS, Sawaya MR, Rettie S, Li X, Antselovich I, Craven TW, Watkins AM, Labonte JW, DiMaio F, Yeates TO, Baker D, Computational design of mixed chirality peptide macrocycles with internal symmetry. Protein Sci. 29, 2433–2445 (2020). [PubMed: 33058266]
16. Wei KY, Moschidi D, Bick MJ, Nerli S, McShan AC, Carter LP, Huang P-S, Fletcher DA, Sgourakis NG, Boyken SE, Baker D, Computational design of closely related proteins that adopt two well-defined but structurally divergent folds. Proc. Natl. Acad. Sci. U. S. A 117, 7208–7215 (2020). [PubMed: 32188784]
17. Langan RA, Boyken SE, Ng AH, Samson JA, Dods G, Westbrook AM, Nguyen TH, Lajoie MJ, Chen Z, Berger S, Mulligan VK, Dueber JE, Novak WRP, El-Samad H, Baker D, De novo design of bioactive protein switches. Nature. 572, 205–210 (2019). [PubMed: 31341284]
18. Quijano-Rubio A, Yeh H-W, Park J, Lee H, Langan RA, Boyken SE, Lajoie MJ, Cao L, Chow CM, Miranda MC, Wi J, Hong HJ, Stewart L, Oh B-H, Baker D, De novo design of modular and tunable protein biosensors. Nature. 591, 482–487 (2021). [PubMed: 33503651]
19. Zhang JZ, Yeh H-W, Walls AC, Wicky BIM, Sprouse KR, VanBlargan LA, Treger R, Quijano-Rubio A, Pham MN, Kraft JC, Haydon IC, Yang W, DeWitt M, Bowen JE, Chow CM, Carter L, Ravichandran R, Wener MH, Stewart L, Veesler D, Diamond MS, Greninger AL, Koelle DM, Baker D, Thermodynamically coupled biosensors for detecting neutralizing antibodies against SARS-CoV-2 variants. Nat. Biotechnol 40, 1336–1340 (2022). [PubMed: 35484405]
20. Wang M, Guo Q, Zhu K, Fang B, Yang Y, Teng M, Li X, Tao Y, Interface switch mediates signal transmission in a two-component system. Proceedings of the National Academy of Sciences. 117, 30433–30440 (2020).
21. Brunette TJ, Parmeggiani F, Huang P-S, Bhabha G, Ekiert DC, Tsutakawa SE, Hura GL, Tainer JA, Baker D, Exploring the repeat protein universe through computational protein design. Nature. 528, 580–584 (2015). [PubMed: 26675729]
22. Brunette TJ, Bick MJ, Hansen JM, Chow CM, Kollman JM, Baker D, Modular repeat protein sculpting using rigid helical junctions. Proc. Natl. Acad. Sci. U. S. A 117, 8870–8875 (2020). [PubMed: 32245816]
23. Khatib F, Cooper S, Tyka MD, Xu K, Makedon I, Popovic Z, Baker D, Players F, Algorithm discovery by protein folding game players. Proc. Natl. Acad. Sci. U. S. A 108, 18949–18953 (2011). [PubMed: 22065763]
24. Tyka MD, Keedy DA, André I, Dimaio F, Song Y, Richardson DC, Richardson JS, Baker D, Alternate states of proteins revealed by detailed energy landscape mapping. J. Mol. Biol 405, 607–618 (2011). [PubMed: 21073878]
25. Koga N, Tatsumi-Koga R, Liu G, Xiao R, Acton TB, Montelione GT, Baker D, Principles for designing ideal protein structures. Nature. 491, 222–227 (2012). [PubMed: 23135467]
26. Lin Y-R, Koga N, Tatsumi-Koga R, Liu G, Clouser AF, Montelione GT, Baker D, Control over overall shape and size in de novo designed proteins. Proc. Natl. Acad. Sci. U. S. A 112, E5478–85 (2015). [PubMed: 26396255]
27. Dauparas J, Anishchenko I, Bennett N, Bai H, Ragotte RJ, Milles LF, Wicky BIM, Courbet A, de Haas RJ, Bethel N, Leung PJY, Huddy TF, Pellock S, Tischer D, Chan F, Koepnick B, Nguyen H, Kang A, Sankaran B, Bera AK, King NP, Baker D, Robust deep learning–based protein sequence design using ProteinMPNN. Science. 378, 49–56 (2022). [PubMed: 36108050]
28. Jumper J, Evans R, Pritzel A, Green T, Figurnov M, Ronneberger O, Tunyasuvunakool K, Bates R, Žídek A, Potapenko A, Bridgland A, Meyer C, Kohl SAA, Ballard AJ, Cowie A, Romera-Paredes B, Nikolov S, Jain R, Adler J, Back T, Petersen S, Reiman D, Clancy E, Zielinski M, Steinegger M, Pacholska M, Berghammer T, Bodenstein S, Silver D, Vinyals O, Senior AW, Kavukcuoglu K, Kohli P, Hassabis D, Highly accurate protein structure prediction with AlphaFold. Nature. 596, 583–589 (2021). [PubMed: 34265844]

29. Bennett N, Coventry B, Goreshnik I, Huang B, Allen A, Vafeados D, Peng YP, Dauparas J, Baek M, Stewart L, DiMaio F, De Munck S, Savvides SN, Baker D, Improving de novo Protein Binder Design with Deep Learning. bioRxiv (2022), p. 2022.06.15.495993, , doi:10.1101/2022.06.15.495993.
30. Cao L, Coventry B, Goreshnik I, Huang B, Sheffler W, Park JS, Jude KM, Marković I, Kadam RU, Verschueren KHG, Verstraete K, Walsh STR, Bennett N, Phal A, Yang A, Kozodoy L, DeWitt M, Picton L, Miller L, Strauch E-M, DeBouver ND, Pires A, Bera AK, Halabiya S, Hammerson B, Yang W, Bernard S, Stewart L, Wilson IA, Ruohola-Baker H, Schlessinger J, Lee S, Savvides SN, Garcia KC, Baker D, Design of protein-binding proteins from the target structure alone. Nature. 605, 551–560 (2022). [PubMed: 35332283]
31. Berliner, Hankovszky Olga, A Novel Reversible Thiol-Specific Spin Label: Papain Active Site Labeling and Inhibition'. Anal. Biochem
32. Tessmer MH, Stoll S, chiLife: An open-source Python package for in silico spin labeling and integrative protein modeling. bioRxiv (2022), p. 2022.12.23.521725, , doi:10.1101/2022.12.23.521725.
33. Wang J, Lisanza S, Juergens D, Tischer D, Watson JL, Castro KM, Ragotte R, Saragovi A, Milles LF, Baek M, Anishchenko I, Yang W, Hicks DR, Expòsit M, Schlichthaerle T, Chun J-H, Dauparas J, Bennett N, Wicky BIM, Muenks A, DiMaio F, Correia B, Ovchinnikov S, Baker D, Scaffolding protein functional sites using deep learning. Science. 377, 387–394 (2022). [PubMed: 35862514]
34. Baek M, DiMaio F, Anishchenko I, Dauparas J, Ovchinnikov S, Lee GR, Wang J, Cong Q, Kinch LN, Schaeffer RD, Millán C, Park H, Adams C, Glassman CR, DeGiovanni A, Pereira JH, Rodrigues AV, van Dijk AA, Ebrecht AC, Opperman DJ, Sagmeister T, Buhlheller C, Pavkov-Keller T, Rathinaswamy MK, Dalwadi U, Yip CK, Burke JE, Garcia KC, Grishin NV, Adams PD, Read RJ, Baker D, Accurate prediction of protein structures and interactions using a three-track neural network. Science. 373, 871–876 (2021). [PubMed: 34282049]
35. Hallinan JP, Doyle LA, Shen BW, Gewe MM, Takushi B, Kennedy MA, Friend D, Roberts JM, Bradley P, Stoddard BL, Design of functionalised circular tandem repeat proteins with longer repeat topologies and enhanced subunit contact surfaces. Commun Biol. 4, 1240 (2021). [PubMed: 34716407]
36. Kibler RD, Lee S, Kennedy MA, Wicky BIM, Lai SM, Kostelic MM, Li X, Chow CM, Carter L, Wysocki VH, Stoddard BL, Baker D, Stepwise design of pseudosymmetric protein hetero-oligomers. bioRxiv (2023), p. 2023.04.07.535760, , doi:10.1101/2023.04.07.535760.
37. Sahtoe DD, Praetorius F, Courbet A, Hsia Y, Wicky BIM, Edman NI, Miller LM, Timmermans BJR, Decarreau J, Morris HM, Kang A, Bera AK, Baker D, Reconfigurable asymmetric protein assemblies through implicit negative design. Science. 375, eabj7662 (2022). [PubMed: 35050655]
38. Crooks GE, Hon G, Chandonia J-M, Brenner SE, WebLogo: a sequence logo generator. Genome Res. 14, 1188–1190 (2004). [PubMed: 15173120]
39. Wu K, Bai H, Chang Y-T, Redler R, McNally KE, Sheffler W, Brunette TJ, Hicks DR, Morgan TE, Stevens TJ, Broerman A, Goreshnik I, DeWitt M, Chow CM, Shen Y, Stewart L, Derivery E, Silva DA, Bhabha G, Ekiert DC, Baker D, De novo design of modular peptide-binding proteins by superhelical matching. Nature (2023), doi:10.1038/s41586-023-05909-9.
40. Torres SV, Leung PJY, Lutz ID, Venkatesh P, Watson JL, Hink F, Huynh H-H, Yeh AH-W, Juergens D, Bennett NR, Hoofnagle AN, Huang E, MacCoss MJ, Expòsit M, Lee GR, Korkmaz EN, Nivala J, Stewart L, Rodgers JM, Baker D, De novo design of high-affinity protein binders to bioactive helical peptides. bioRxiv (2022), p. 2022.12.10.519862, , doi:10.1101/2022.12.10.519862.
41. Praetorius Florian, Leung Philip J. Y., Tessmer Maxx H., Broerman Adam, Demakis Cullen, Idris Abbas, Stoll Stefan, and Baker David, Data for Design of stimulus-responsive two-state hinge proteins. Zenodo, , doi:10.5281/zenodo.8122343.
42. Alford RF, Leaver-Fay A, Jeliazkov JR, O'Meara MJ, DiMaio FP, Park H, Shapovalov MV, Renfrew PD, Mulligan VK, Kappel K, Labonte JW, Pacella MS, Bonneau R, Bradley P, Dunbrack RL Jr, Das R, Baker D, Kuhlman B, Kortemme T, Gray JJ, The Rosetta All-Atom Energy Function for Macromolecular Modeling and Design. J. Chem. Theory Comput 13, 3031–3048 (2017). [PubMed: 28430426]

43. An L, Lee GR, De Novo Protein Design Using the Blueprint Builder in Rosetta. Curr. Protoc. Protein Sci 102, e116 (2020). [PubMed: 33320432]
44. Sauer MF, Sevy AM, Crowe JE Jr, Meiler J, Multi-state design of flexible proteins predicts sequences optimal for conformational change. PLoS Comput. Biol 16, e1007339 (2020). [PubMed: 32032348]
45. Chennamsetty N, Voynov V, Kayser V, Helk B, Trout BL, Design of therapeutic proteins with enhanced stability. Proc. Natl. Acad. Sci. U. S. A 106, 11937–11942 (2009). [PubMed: 19571001]
46. Warszawski S, Netzer R, Tawfik DS, Fleishman SJ, A “fuzzy”-logic language for encoding multiple physical traits in biomolecules. J. Mol. Biol 426, 4125–4138 (2014). [PubMed: 25311857]
47. Kudlacek ST, Metz S, Thiono D, Payne AM, Phan TTN, Tian S, Forsberg LJ, Maguire J, Seim I, Zhang S, Tripathy A, Harrison J, Nicely NI, Soman S, McCracken MK, Gromowski GD, Jarman RG, Premkumar L, de Silva AM, Kuhlman B, Designed, highly expressing, thermostable dengue virus 2 envelope protein dimers elicit quaternary epitope antibodies. Sci. Adv 7, eabg4084 (2021). [PubMed: 34652943]
48. Wicky BIM, Milles LF, Courbet A, Ragotte RJ, Dauparas J, Kinfu E, Tipps S, Kibler RD, Baek M, DiMaio F, Li X, Carter L, Kang A, Nguyen H, Bera AK, Baker D, Hallucinating symmetric protein assemblies. Science. 378, 56–61 (2022). [PubMed: 36108048]
49. Mirdita M, Schütze K, Moriwaki Y, Heo L, Ovchinnikov S, Steinegger M, ColabFold: making protein folding accessible to all. Nat. Methods 19, 679–682 (2022). [PubMed: 35637307]
50. Lauer TM, Agrawal NJ, Chennamsetty N, Egodage K, Helk B, Trout BL, Developability index: a rapid in silico tool for the screening of antibody aggregation propensity. J. Pharm. Sci 101, 102–115 (2012). [PubMed: 21935950]
51. Yao S, Moyer A, Zheng Y, Shen Y, Meng X, Yuan C, Zhao Y, Yao H, Baker D, Wu C, De novo design and directed folding of disulfide-bridged peptide heterodimers. Nat. Commun 13, 1539 (2022). [PubMed: 35318337]
52. Dang B, Mravic M, Hu H, Schmidt N, Mensa B, DeGrado WF, SNAC-tag for sequence-specific chemical protein cleavage. Nat. Methods 16, 319–322 (2019). [PubMed: 30923372]
53. Virtanen P, Gommers R, Oliphant TE, Haberland M, Reddy T, Cournapeau D, Burovski E, Peterson P, Weckesser W, Bright J, van der Walt SJ, Brett M, Wilson J, Millman KJ, Mayorov N, Nelson ARJ, Jones E, Kern R, Larson E, Carey CJ, Polat İ, Feng Y, Moore EW, VanderPlas J, Laxalde D, Perktold J, Cimrman R, Henriksen I, Quintero EA, Harris CR, Archibald AM, Ribeiro AH, Pedregosa F, van Mulbregt P, SciPy 1.0 Contributors, SciPy 1.0: fundamental algorithms for scientific computing in Python. Nat. Methods 17, 261–272 (2020). [PubMed: 32015543]
54. Tessmer MH, Canarie ER, Stoll S, Comparative evaluation of spin-label modeling methods for protein structural studies. Biophys. J 121, 3508–3519 (2022). [PubMed: 35957530]
55. Polyhach Y, Bordignon E, Jeschke G, Rotamer libraries of spin labelled cysteines for protein studies. Phys. Chem. Chem. Phys 13, 2356–2366 (2011). [PubMed: 21116569]
56. Stoll S, Schweiger A, EasySpin, a comprehensive software package for spectral simulation and analysis in EPR. J. Magn. Reson 178, 42–55 (2006). [PubMed: 16188474]
57. Fábregas Ibáñez L, Jeschke G, Stoll S, DeerLab: a comprehensive software package for analyzing dipolar electron paramagnetic resonance spectroscopy data. Magn Reson (Gott). 1, 209–224 (2020). [PubMed: 34568875]
58. Fábregas-Ibáñez L, Jeschke G, Stoll S, Compactness regularization in the analysis of dipolar EPR spectroscopy data. J. Magn. Reson 339, 107218 (2022). [PubMed: 35439683]
59. Kabsch W, XDS. Acta Crystallogr. D Biol. Crystallogr 66, 125–132 (2010). [PubMed: 20124692]
60. Winn MD, Ballard CC, Cowtan KD, Dodson EJ, Emsley P, Evans PR, Keegan RM, Krissinel EB, Leslie AGW, McCoy A, McNicholas SJ, Murshudov GN, Pannu NS, Potterton EA, Powell HR, Read RJ, Vagin A, Wilson KS, Overview of the CCP4 suite and current developments. Acta Crystallogr. D Biol. Crystallogr 67, 235–242 (2011). [PubMed: 21460441]
61. McCoy AJ, Grosse-Kunstleve RW, Adams PD, Winn MD, Storoni LC, Read RJ, Phaser crystallographic software. J. Appl. Crystallogr 40, 658–674 (2007). [PubMed: 19461840]
62. Adams PD, Afonine PV, Bunkóczi G, Chen VB, Davis IW, Echols N, Headd JJ, Hung L-W, Kapral GJ, Grosse-Kunstleve RW, McCoy AJ, Moriarty NW, Oeffner R, Read RJ, Richardson

DC, Richardson JS, Terwilliger TC, Zwart PH, PHENIX: a comprehensive Python-based system for macromolecular structure solution. Acta Crystallogr. D Biol. Crystallogr 66, 213–221 (2010). [PubMed: 20124702]

63. Emsley P, Cowtan K, Coot: model-building tools for molecular graphics. Acta Crystallogr. D Biol. Crystallogr 60, 2126–2132 (2004). [PubMed: 15572765]
64. Williams CJ, Headd JJ, Moriarty NW, Prisant MG, Videau LL, Deis LN, Verma V, Keedy DA, Hintze BJ, Chen VB, Jain S, Lewis SM, Arendall III WB, Snoeyink J, Adams PD, Lovell SC, Richardson JS, Richardson DC, MolProbity: More and better reference data for improved all-atom structure validation. Protein Sci. 27, 293–315 (2018). [PubMed: 29067766]

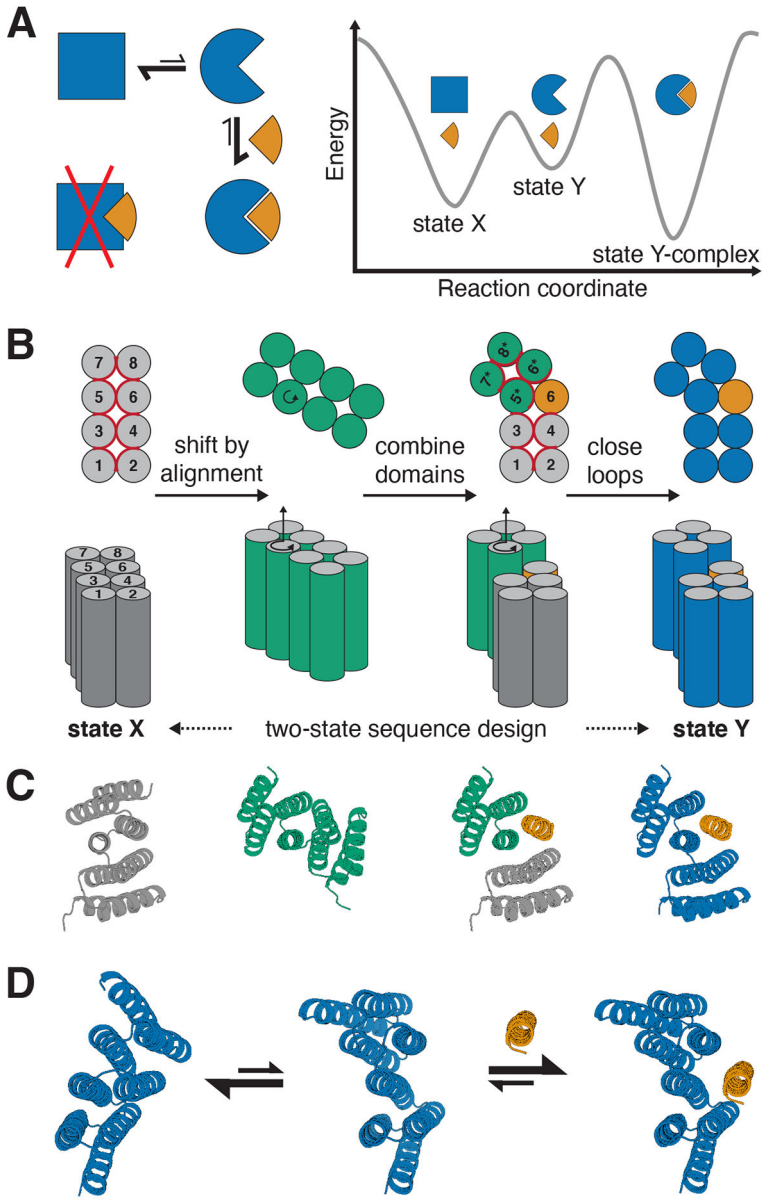

Figure 1: Strategy for designing proteins that can switch between different conformations.

A) Left: reaction scheme for a protein (blue) that undergoes a conformational change and can bind an effector (orange) in one (circle) but not in the other conformational state (square). Right: Energy landscape for the system shown on the left. **B)** Schematic representation of the hinge design approach. Alpha-helices are represented as circles (top view, top) or cylinders (side view, bottom). From left to right: A previously designed repeat protein (gray) serves as the first conformation of the hinge. To generate the second conformation a copy of the repeat protein (green) is moved by shifted alignment along a pivot helix, causing a rotation (top and bottom, indicated by circular arrow) and a translation along the helix axis (bottom). The first 4 helices of the original protein form domain 1 of the hinge, the last 4 helices of the rotated copy form domain 2, and an additional helix is copied over from the original protein to serve as an effector peptide (orange) that can bind

to this second conformation of the hinge. Both domains of the hinge are connected into one continuous chain (blue) using fragment-based loop closure, and a single amino acid sequence is designed to be compatible with both conformations. **C)** Design steps from B illustrated using cartoon representations of an exemplary design trajectory. **D)** Exemplary design models of a designed hinge protein in state X (left), state Y (center), and in state Y bound to an effector peptide (right). Hinge is shown in blue, peptide in orange.

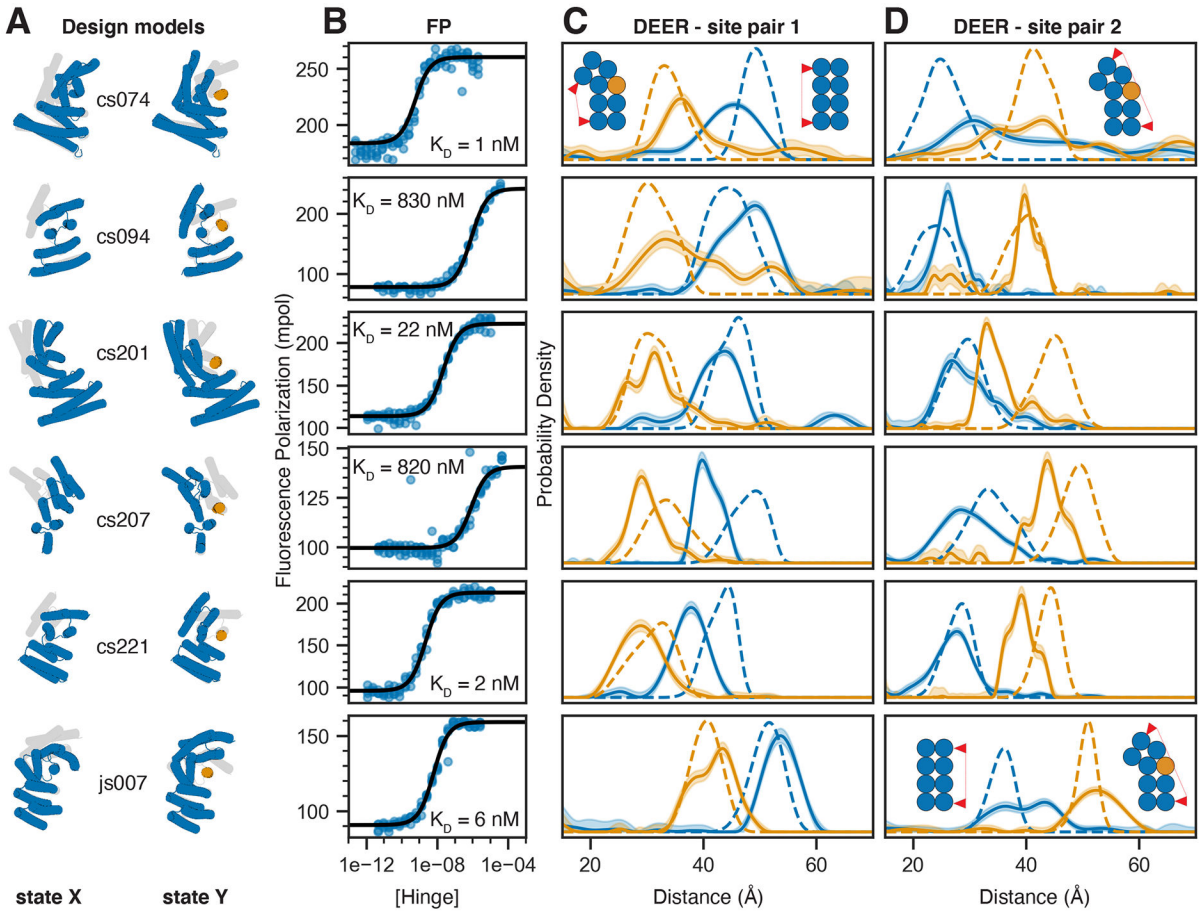

Figure 2: Experimental validation of peptide-binding hinges.

A) Design models of hinges (blue) and peptides (orange) in state X (left model) and state Y bound to the peptide (right model). Gray shades behind models in state X and Y indicate the corresponding states Y and X, respectively. **B)** Fluorescence Polarization (FP) titrations with a constant concentration of TAMRA-labeled peptide (0.1 nM for cs074 and cs221; 0.5 nM for cs201; 1 nM for cs094, cs207, and js007) and varying hinge concentrations. Circles represent data points from four independent measurements, lines are fits of standard binding isotherms to all data points, dissociation constants (K_D) are obtained from those fits. **C,D)** Distance distributions between spin labels covalently attached to cysteine side chains. Solid lines are obtained from DEER experiments without (blue) or with (orange) an excess of peptide, shaded areas are 95% confidence intervals, and dashed lines are simulated based on the design models for state X (blue) or the state Y complex (orange). For each hinge two different label site pairs were tested, one in which the distance was expected to decrease with peptide binding (C) and one in which the distance was expected to increase upon peptide binding (D). Chemically synthesized peptides were used for all measurements except for cs074 site pair 1, for which sfGFP-peptide fusion was used. For design cs094, the residual state X peak in presence of the peptide can be explained by incomplete binding either due to weak binding affinity or to insufficient peptide concentration.

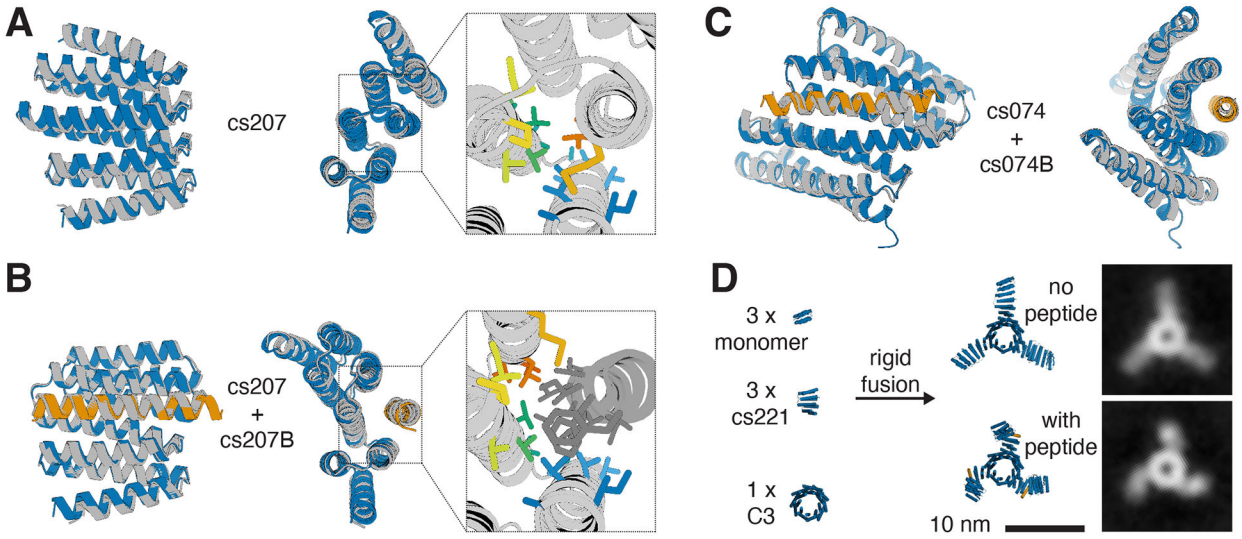

Figure 3: Close agreement between crystal structures and design models for both designed states.

A) Design model (blue) of hinge cs207 in state X overlaid with crystal structure (gray) of hinge cs207 crystallized without peptide. Right panel shows a close-up view of the side chains in the interface between the two hinge domains (side chain colors follow a spectrum from blue to red from N- to C- terminus). **B)** Design model (hinge in blue, peptide in orange) of the cs207 state Y hinge-peptide complex overlaid with crystal structure (gray) of hinge cs207 co-crystallized with peptide cs207B. Right panel shows a close-up view of the side chains in the interface between hinge and peptide (hinge side chain colors match the corresponding side chains in A, peptide side chains are shown in dark gray). **C)** Design model (hinge in blue, peptide in orange) of hinge cs074 in state Y overlaid with crystal structure (gray) of hinge cs074 co-crystallized with peptide cs207B. Representative electron densities for all crystal structures are shown in Figure S19. RMSD values between design model and experimental structure are given in Table S4. **D)** Left: Components for design of a C3-symmetric homotrimer with three cs221 hinge arms. Center: Design model of the hinge-armed trimer in state X (top) and in state Y (bottom). Right: nsEM class averages of the trimer in absence of peptide (top) and in presence (bottom) of peptide cs221B.

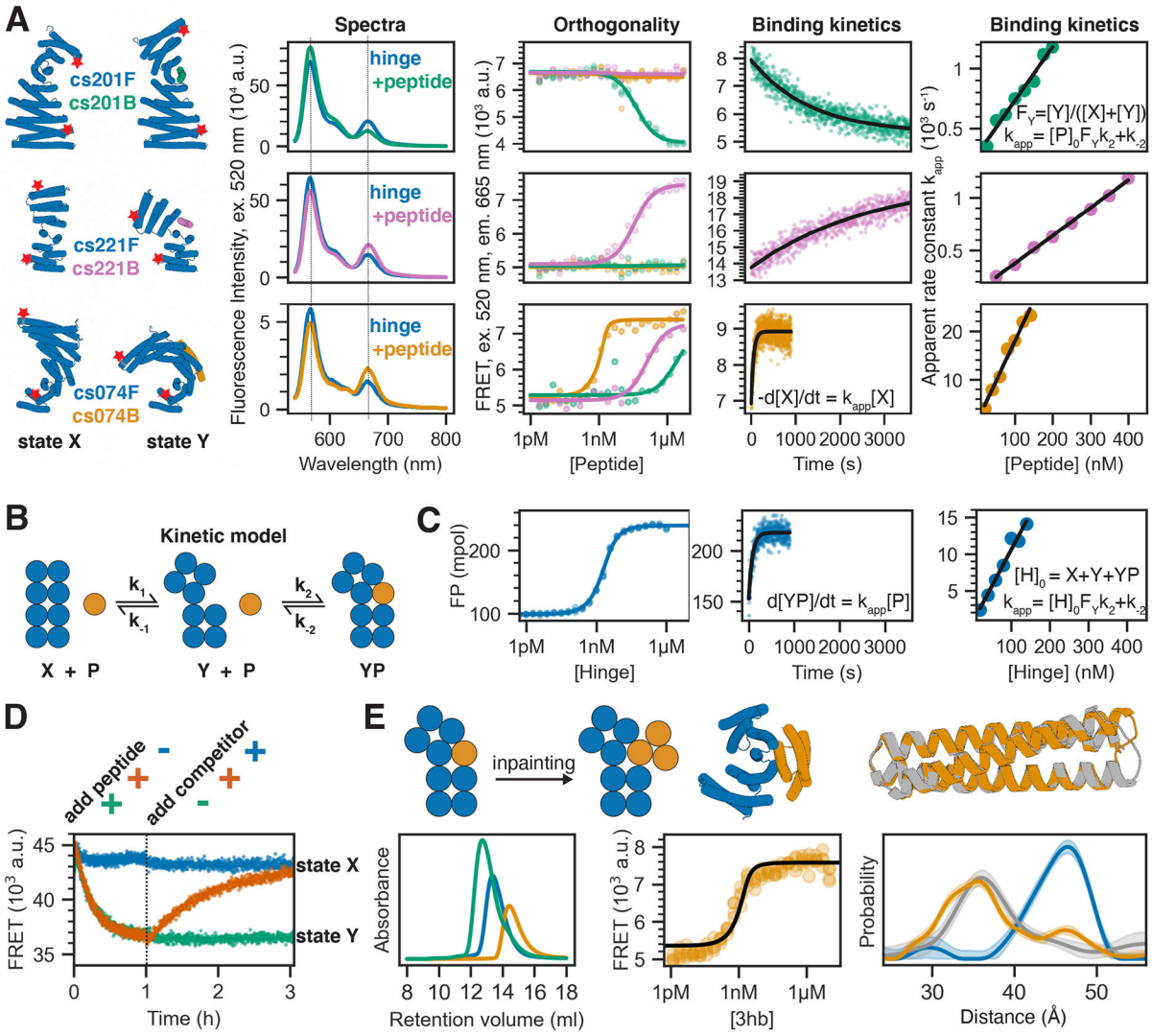

Figure 4: Quantitative analysis of conformational changes in designed hinge proteins

A) FRET-based characterization of three extended hinges. From left to right: cylindrical representation of extended hinges (blue) and their corresponding target peptides (green: cs201B, pink: cs221B, orange: cs074B) with red stars indicating attachment sites for fluorescent dyes; fluorescence spectra (excitation at 520 nm) of labeled hinge without (blue) or with (green/pink/orange) target peptide; FRET-based binding titrations (excitation 520 nm, emission 665 nm) at 2 nM labeled hinge and varying peptide concentrations fitted with standard binding isotherms (solid lines); time course after mixing 2 nM (cs201F, cs074F) or 5 nM (cs221F) labeled hinge and 100 nM peptide fitted with a single-exponential equation (black line); apparent rate constants obtained from single-exponential kinetic fits plotted against absolute peptide concentrations (circles) and fitted with a linear equation (black line). Dotted lines in spectra indicate acceptor and donor emission peaks. **B)** Kinetic model describing the coupling of the conformational equilibrium to the binding equilibrium. X and Y: hinge in state X and Y, respectively; P: peptide; YP: peptide bound to hinge in state Y. k_1, k_{-1}, k_2, and k_{-2} are the microscopic rate constants. **C)** FP characterization of unlabeled

extended hinge cs074F. From left to right: binding titration at 0.1 nM TAMRA-labeled peptide and varying hinge concentrations; time course after mixing 2 nM TAMRA-labeled peptide and 100 nM hinge fitted with a single-exponential equation (black line); apparent rate constants obtained from single-exponential kinetic fits plotted against absolute hinge concentrations (circles) and fitted with a linear equation (black line). **D)** FRET-based reversibility experiment using the labeled extended hinge cs201F introduced in C). Hinge concentration is 30 nM for all traces; 1 μM peptide is added at t=0 (green/orange), 3 μM unlabeled competitor hinge is added after 1 h (blue/orange). **E)** Top from left to right: schematic representation of the inpainting procedure that adds two helices to the peptide cs074B yielding a three-helix bundle (3hb); cylindrical representation of 3hb_05(orange) bound to hinge cs074 (blue); overlay of design model (orange) and crystal structure (gray) of 3hb_05. Bottom from left to right: SEC traces for hinge cs074 (blue), 3hb_05 (orange), and a mixture of both (green); FRET-based titration of 2 nM extended labeled hinge cs074F and varying concentrations of 3hb_05 fitted with a standard binding isotherm (back line); Distance distributions obtained from DEER experiments as described in Figure 2 (blue: cs074, gray: cs074 + peptide cs074B, orange: cs074 + 3hb_05).

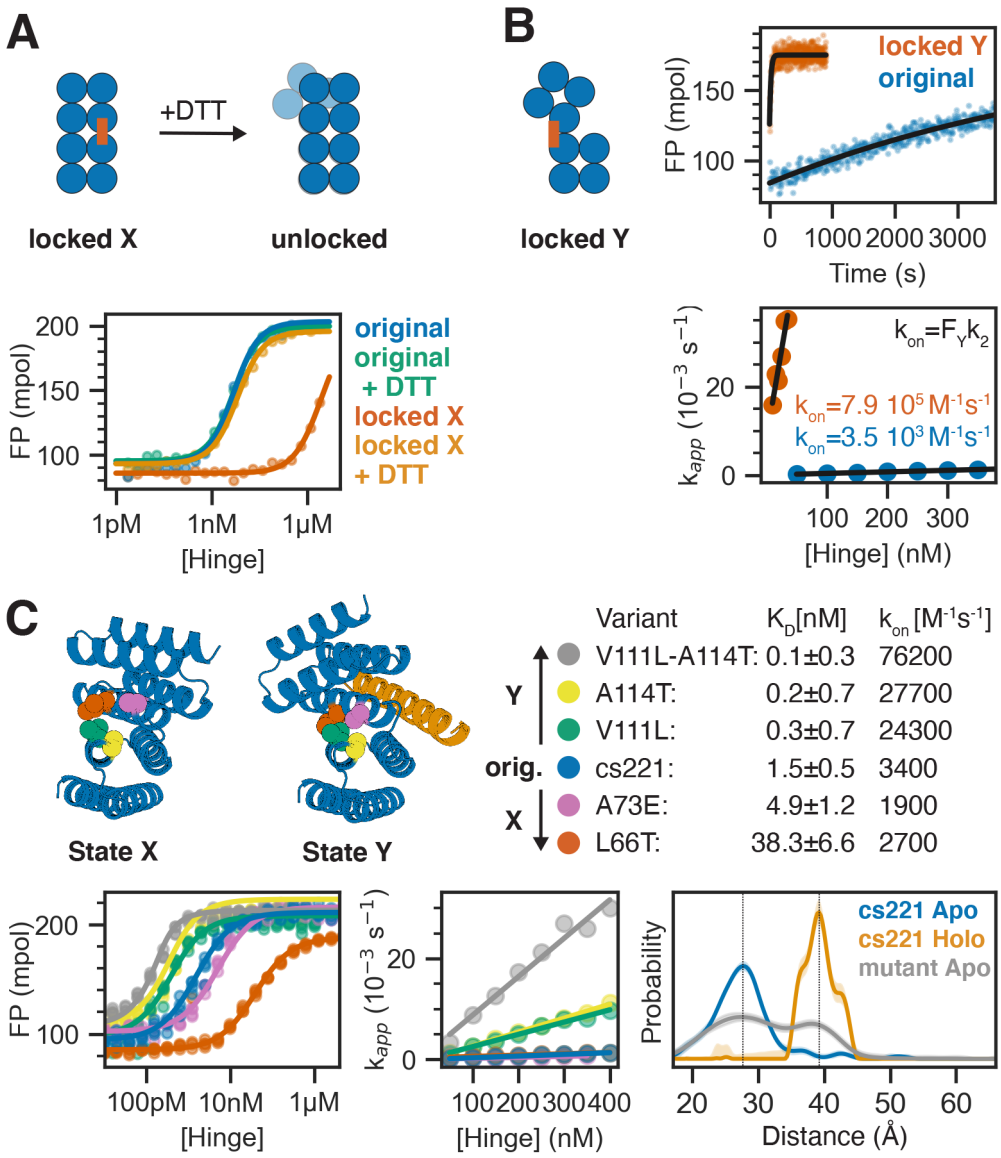

Figure 5: Controlling the conformational pre-equilibrium affects peptide binding.

A) Left: Schematic representation of a hinge containing two cysteine residues that can form a disulfide bond in state X but not in state Y, effectively locking the hinge in state X under oxidizing conditions. Upon addition of reducing agent DTT the disulfide bond is broken and the conformational equilibrium is restored. Right: FP-based titration of 1 nM TAMRA-labeled peptide and a hinge with state X disulfide (red, orange) or the parent hinge without cysteines (blue, green) under oxidizing (blue, red) or reducing (green, orange) conditions. **B)** From left to right: schematic representation of a hinge that is disulfide-locked in state Y; time course after mixing 2 nM TAMRA-labeled peptide and 50 nM locked hinge (red) or original hinge without cysteines (blue) fitted with a single-exponential equation (black line); apparent rate constants obtained from single-exponential kinetic fits plotted against absolute hinge concentrations (circles) and fitted with a linear equation (black line). **C)** Tuning the pre-equilibrium with point mutations. Top left: Cartoon representation of

hinge cs221 highlighting positions of point mutations. Top right: Dissociation constants (K_D) and observed binding rate constants (k_{on}). Bottom left: FP-based titration of 0.1 nM (yellow, green, blue) or 1 nM (pink, red) TAMRA-labeled peptide cs221B and varying concentrations of hinge variants containing one or two point mutations. Bottom center: Apparent rate constants obtained from single-exponential kinetic fits plotted against absolute hinge concentrations (circles) and fitted with a linear equation (black line). Bottom right: DEER distance distribution for the double mutant cs221-V111L-A114T in absence of peptide (gray) in comparison to the original cs221 with (orange) and without (blue) peptide. Vertical lines serve as guide to the eye indicating state X and state Y distances.